Chapter 3

The Central Calorimeter

The central calorimeter consists of 1280 counters, which are F2 lead-glass blocks with an attached photomultiplier tube. The central calorimeter is designed to measure the energy deposited by electromagnetic showers induced by incident electrons, positrons and gamma rays. Below are sections devoted to design criteria, quality control and construction. The calibration of the central calorimeter is discussed in chapter 4.

3.1 Requirements and Design

The physics that is being investigated determines the type of experimental apparatus that is needed. The central calorimeter is designed to search for specific physics signals of interest while being able to identify background signals.

3.1.1 Physics criteria

The basic charmonium signal that E760 is sensitive to is the e^+e^- decay of J/ψ. The calorimeter measurement of the energies and positions of the two decay particles has to be made good enough to reconstruct the correct invariant mass. The measurements depend on calibration (chapter 4) and the inherent properties of the calorimeter. If the counters are too large then the position resolution becomes poor. On the other hand, if the counters are too small then the energy measurement resolution will be degraded; smaller counters imply a larger number of channels which increases the cost.

E760 is also designed to look for final states of two and three gamma rays (χ_2, η_c, $\eta_c' \rightarrow \gamma\gamma$ and ${}^1\mathrm{P}_1 \rightarrow \gamma\eta_c \rightarrow \gamma\gamma\gamma$). The main expected background comes from $n\pi^o$, in particular $\pi^o\pi^o$. A symmetric decay of an energetic π^o will result in both photons inducing electromagnetic showers close to one another. It is important to be able to identify π^o energy deposits. If the counters are too large, then the two showers will appear as one incident particle. The granularity of the calorimeter has to be able to determine when there are two incident particles near each other as in symmetric π^o decays. Asymmetric π^o decays will have a low energy photon. This photon can escape detection by either being below the calorimeter threshold or by missing the apparatus ($\theta_{lab} > 70°$). The acceptance of the detector cannot be increased because of the space taken up by the gas jet apparatus. Hence, the threshold was a crucial consideration in the design of the calorimeter. The counters must have a low energy

Figure 3.1: The design of the central calorimeter with twenty different shaped blocks and their orientation to the interaction region.

detection threshold and accurately measure the large energy deposits of two body final states.

The calorimeter acceptance is determined in the backward direction by the gas jet apparatus. Physics considerations and radiation damage properties of the lead-glass determine the forward acceptance cutoff of the calorimeter. The high background interaction rate is forward peaked; exposure of the lead-glass to this high rate was a consideration. Also a significant fraction of the charmonium decays with high invariant mass e^+e^- pairs can be contained in the region $15° < \theta < 70°$ (as covered by the threshold Čerenkov detector, section 2.5). Therefore, the central calorimeter does not need to cover much of the region forward of 15°. However the detection of other particles in the final state (radiative gamma rays and pions from hadronic decays) is desirable to fully contain the events and to be able to do exclusive fits. The final calorimeter acceptance chosen is polar angles from 10° to 70° and the full azimuth.

Block or Shape Number	Length (cm)	Central θ (degree)	$\Delta\theta$ (degree)	Distance from target (cm)	PMT Size (in)	Fractional PMT Coverage
1	37.80	67.387	5.226	72.44	3.0	0.473
2	38.65	62.259	5.031	75.87	3.0	0.475
3	39.88	57.342	4.803	80.07	3.0	0.476
4	41.50	52.664	4.552	85.08	3.0	0.478
5	43.54	48.246	4.284	90.96	3.0	0.479
6	46.03	44.101	4.007	97.79	3.0	0.481
7	48.98	40.234	3.728	105.62	3.0	0.482
8	50.00	36.644	3.451	114.54	3.0	0.497
9	50.00	33.327	3.183	124.66	3.0	0.520
10	50.00	30.273	2.925	136.07	3.0	0.544
11	50.00	27.472	2.679	148.89	3.0	0.568
12	50.00	24.908	2.449	163.26	3.0	0.593
13	50.00	22.567	2.233	179.34	3.0	0.617
14	50.00	20.434	2.033	197.28	3.0	0.641
15	50.00	18.493	1.848	197.29	2.5	0.546
16	50.00	16.730	1.678	197.29	2.5	0.664
17	50.00	15.130	1.522	197.30	2.0	0.527
18	50.00	13.679	1.380	197.30	2.0	0.644
19	50.00	12.364	1.250	197.30	1.5	0.443
20	50.00	11.174	1.131	197.30	1.5	0.543

Table 3.1: Central calorimeter counters' dimensions and positions; θ is the polar angle. The distance from the target is from the front face of the block to the interaction region. The fractional PMT coverage is the ratio of the areas of the PMT face (the diameter is the PMT size) and the back face of the block.

The forward region (polar angles less than 10°) is covered by the more radiation hard forward calorimeter (section 2.7).

After the material for the central calorimeter was selected (see next section), a Monte Carlo simulation was used to determine the granularity needed to separate symmetrical π^{o} decays. The final segmentation is 64-fold in the azimuth and 20-fold in the polar angle. Each block points back to the interaction region. The polar segmentation thus requires twenty different sizes of blocks which are the shape known as an "erect pyramidal frustum with a regular trapezoidal base". The shapes are numbered 1 to 20 going from polar angles 70° to 10° as seen in figure 3.1. The blocks subtend polar angles varying between 1.1° and 5.2° as seen in table 3.1. Each block subtends 5.6° of the azimuthal angle. Counters at the same azimuthal angle constitute a *wedge* while counters of the same shape and located at the same polar angle are considered a *ring*.

3.1.2 Block Criteria

The correct balance between detection threshold, energy range, energy and position resolution, number of channels, radiation hardness, and cost had to be reached. Materials considered were CsI, NaI, BaF_2, BGO, lead-scintillator fibers and lead-glass. Cost, handling and relative ease of manufacture of the counters lead to the choice of lead-glass. The responses of five types of lead-glass were compared using low energy γ's at the University of Illinois Nuclear Physics Laboratory Tagged Photon Facility. F2 lead-glass was found to have twice as much light output as SF5 glass. This is attributed to the longer path length of shower electrons and greater light transmission. The F2 lead-glass radiation length is 3.14 cm versus 2.54 cm for SF5 glass, which means that for the same amount of shower containment, the F2 lead glass has to be 24% longer. The trade off is that the radiation length is greater and F2 lead-glass does not have as good radiation damage properties as the SF5 glass. The radiation damage properties were studied by exposing both types of glass to radiation doses of ^{137}Cs γ's. The transmission of 400 nm light through 40 cm blocks was decreased by a factor

Element Composition	Percentage by Weight
Lead	42.2
Silicon	21.4
Oxygen	29.5
Potassium	4.2
Sodium	2.3
Arsenic	0.15

Table 3.2: F2 lead glass composition.

of 2 at about 300 and 400 rads for the F2 and SF5 blocks, respectively. However, the F2 overall light output, path length, was the deciding factor in its selection for the calorimeter.

The geometrical characteristics of the blocks were discussed in the previous section and are presented in table 3.1. Included in table 3.1 are the block lengths and distances from the interaction point. The blocks vary between 12 and 16 radiation lengths. The first seven block lengths are shorter due to expected smaller energy deposits and the amount of physical space in the experimental area.

The F2 lead-glass chosen is made by Schott Glass Technologies, Inc. The composition of the F2 lead-glass is shown in table 3.2. The radiation length is 3.141 cm and the density is 3.61 g/cm^3. The refractive index is 1.651 at 404.7 nm and the transmission quality of the glass is discussed below in section 3.2.2. The F2 lead-glass was cut and polished by Cosmo Optics, Inc. Each edge of the blocks has a 2 mm chamfer of ground glass finish.

Model Number	Diameter (in)	Length (in)	Number of Dynodes
R3036-02	3.0	5.0	12
R3345-02	2.5	5.0	12
R2154-04	2.0	6.0	10
R580-13	1.5	6.0	10

Table 3.3: The four different photomultiplier tubes' physical characteristics.

3.1.3 Photomultiplier Criteria

The photomultiplier tubes (PMT) need to be able to collect the light efficiently. The PMT's also need a sufficient dynamic linear range from the calorimeter detection threshold to the full energy deposit of a two body final state. The gains of the PMT's also have to be able to drive the electronics involved, i.e. FERA ADC's. Since there are no light guides between the lead-glass blocks and the PMT's, it was not possible to place μ-metal shields beyond the photocathode surfaces. Due to the existence of stray magnetic fields within the accelerator environment, the PMT's have to be insensitive to magnetic fields of up to a few gauss.

PMT's with four different diameters are needed to match the blocks' back face surface areas and to maximize light collection (see table 3.1). Linear focused 3.0 inch PMT's from three manufacturers were tested. The PMT's with good timing precision are generally inferior in light collection, which is important in detecting low energy particles efficiently. Two PMT's, EMI D640 and Hamamatsu R3036, which were specifically manufactured for the experiment, have rise times between 6 and 10 ns and good light collection. E760 chose Hamamatsu tubes on the basis of price.

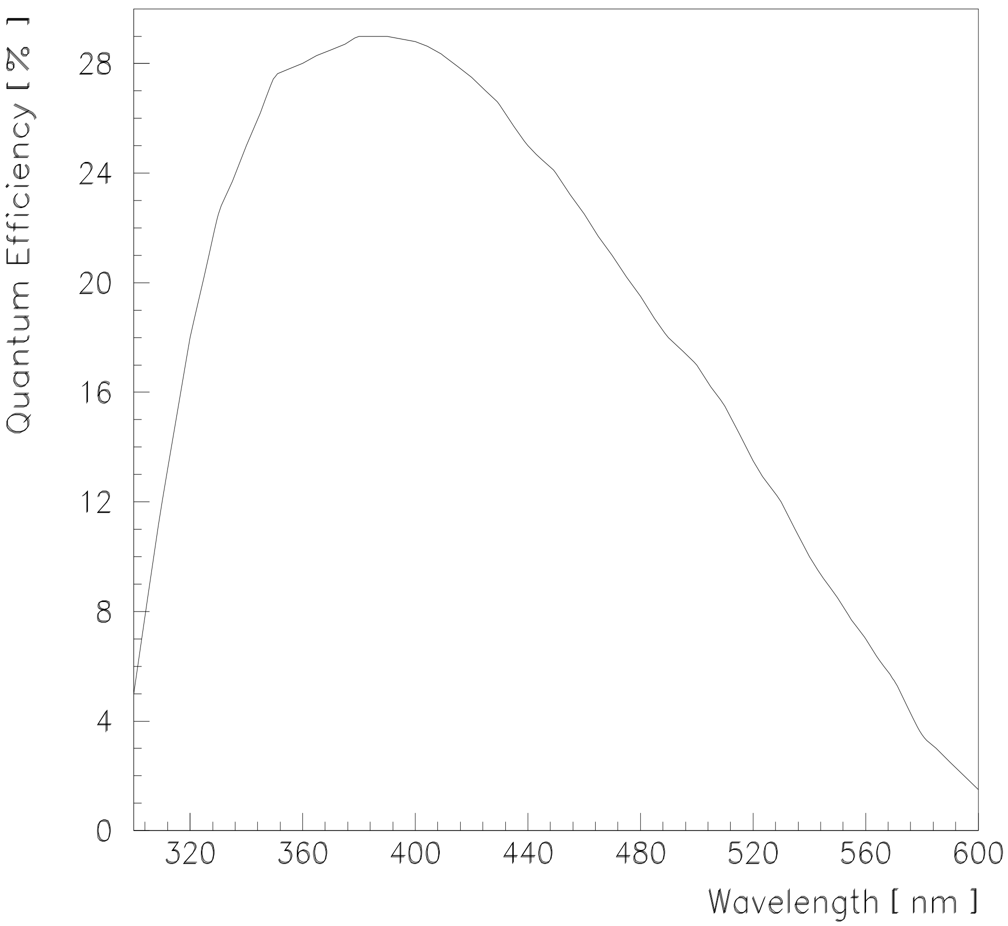

Figure 3.2: The quantum efficiency of the PMT's as a function of wavelength.

The physical characteristics of the four different sized tubes are shown in table 3.3. The PMT's operate with positive high voltage with a bleeder current approximately 200 microamperes. The lengths listed include the base circuit which forms an integral assembly with the PMT. A Bialkali photocathode is coated on a Borosilicate glass window. The sensitive range is between 300 and 650 nm, with the peak sensitivity at 420 nm. Figure 3.2 shows the quantum efficiency of the Hamamatsu PMT's as a function of wavelength.

Figure 3.3: A sketch of a stainless steel wedge unit

3.1.4 Central Calorimeter Support Structure

Each wedge support structure (a *shell*) contains twenty blocks, one of each shape. A wedge unit has to be both mechanically and electrically independent while, ideally, being light tight. Mechanically, a wedge shell has to be able to support the blocks in the correct positions at any angle in azimuth. Electrically, there has to be a way of supplying the operating voltage to the PMT's and a method of transporting the signal to the data acquisition electronics. The units have to be light tight and should ideally contain as little material as possible between the blocks and no gaps.

The entire calorimeter assembly also has to be easily moved and installed onto the beam line.

The wedge assembly unit was chosen to be made of stainless steel. See figure 3.3 for a sketch of one stainless steel wedge unit. The surfaces of the wedge shells (*skins*) are 0.735 mm thick; thin septa (*fins*) of 0.254 mm are located inside the shell creating pockets for the counters. The skins cover 2% of the azimuth; only 0.5% of the polar region covered by the central calorimeter are the fins. The shell surfaces and septa were cut and welded by a laser; this was done by Laser Machining. Stainless steel end plates were also welded at the two ends to complete the pockets containing the end blocks (shapes 1 and 20). Two back panels of black anodized aluminum, which partially absorb escaped Čerenkov light (minimizing crosstalk between counters), allow access to the PMT end of the counters. The downstream back panel has a feed-through plate consisting of a set of block connectors which allow operating voltage and signals to be passed. Included as part of the feed-through plate is a fiber optic feed-through (see sections 3.1.5 and 3.2.4). The front side of the shell is closed off by an opaque PVC panel.

The overall support structure is designed to make each wedge unit serve as a structural element. This means that the blocks serve as structural elements carrying compressive loads. The overall support structure must not add any additional stresses to the lead-glass during movement or transport. Two massive support rings are used to support the wedges. The rings rest on rollers which allows the calorimeter to rotate in ϕ, to bring any wedge to the top for maintenance. The overall support structure is

Figure 3.4: A cut-through view of the central calorimeter attached to the massive support rings and the air caster system assembly (raft).

built with a five air caster system (raft) for movement. The overall raft and support rings are shown in figure 3.4 with a cut away view of the central calorimeter.

3.1.5 Gain Monitoring System

Any electromagnetic calorimeter needs to have its response monitored. Each counter's response to a known signal is needed to monitor the counter's gain. A gain monitoring system has been built into the calorimeter apparatus. The monitoring

Figure 3.5: A sketch of the flashlamp gain monitoring system.

system has to be stable and must not interfere with the calorimeter's ability to detect and measure electromagnetic showers.

The gain monitoring system chosen is a single xenon flashlamp as a light source and plastic polymer fiber optic cables to distribute the light to all counters; the gain monitoring system is sketched in figure 3.5. Each flashlamp pulse is 300 ns and peaks at 400 nm. The light is collected and focused by an elliptical reflector into a rectangular lucite mixing bar (*major mixing bar*). A filter wheel placed between the reflector and mixing bar allows selection of the blue component, green component, or the entire spectrum of the light pulses. The mixing bar uniformly distributes light into sixty-four fiber optic cables (for each wedge) and three cables to monitor

PMT's. The sixty-four fibers are connected to the wedges' fiber optic feed-throughs (section 3.1.4). Inside each wedge, a smaller lucite mixing bar (*minor mixing bar*) distributes the light to twenty fiber optic cables which are connected to the individual counters.

3.2 Quality Control

Before construction of any counter or wedge assembly began, each component was tested. The components tested were the PMT's, lead-glass blocks, the wedge shells and the fiber optic system. This was necessary since most of the construction steps (section 3.3) are not easily reversible. These tests, along with tests during construction, insured a well functioning calorimeter.

3.2.1 Photomultiplier Tubes

Besides making sure that the PMT's worked, a range of operating voltages and a set of gain curves were determined. A test stand was built and used in a darkroom at UCI. The test stand held over forty tubes for testing. The PMT's were exposed to a pulsed green LED and blue flashlamp via reflection from a white diffusing screen. A monitor PMT, which was always in the same position in the test stand, measured the intensity of the light pulses. The relative light output at each position in the test stand was measured by a second monitor PMT. The variation in PMT output pulse height is determined from photoelectron statistics.

Model Number	Photocathode Efficiency (rms/mean)	Voltage-gain Constant (m) (rms/mean)
R3036-02	0.10	0.038
R3345-02	0.14	0.034
R2154-04	0.13	0.027
R580-13	0.13	0.026

Table 3.4: The four different photomultiplier tubes' average variabilities of the photocathode response and voltage-gain constant, m.

After an initial *burn period* at 1800 V, which causes a faulty tube to fail quickly, each tube was subjected to the light pulses. The operating voltage was then adjusted to bring the mean PMT response equal to the stationary monitor PMT pulse height. This was an automated process done iteratively using a thousand pulses before trying a different voltage. Once the *equal response* operating voltages were found, the PMT's were exposed to ten thousand pulses at five operating voltages: the equal response voltage and ± 50 and ± 100 volts. For each PMT and light type, the five data points were then fit by the PMT gain equation,

$$gain = b \times V^m, \tag{3.1}$$

where V is the operating voltage, b and m are constants determined by the fit for each PMT (b, which includes the equal response voltage V_o^{-m}, gives the correct gain units and m relates how the gain varies with voltage). The average variabilities (rms/mean) of the photocathode efficiences and voltage-gain constants m are given in table 3.4 for the four different sized tubes. A PMT was rejected if its variability of either the photocathode efficiency or voltage-gain constants was too different from the average.

Figure 3.6: The response of a 3 inch PMT to a range of intensities. The horizontal axis is charge (pC) and the vertical axis is intensity (arbitrary units). During the experiment, full scale corresponds to 2000 pC.

A PMT could also be rejected if the equal response operating voltage was smaller or larger than the expected range of operating voltage (1000 to 1500 volts).

The response of several of the PMT's to a pulsed laser was studied. A 355 nm pulsed laser beam was split and monitored with one PMT. Each PMT was exposed to different intensities of the pulsed laser beam by using a set of linear polarized filters. The response to a range of intensities, shown in figure 3.6, was found to be nearly linear: not deviating by more than 5 to 8% for the larger intensity exposures (corresponding up to a few thousand pC) from the expected response linearly extrapolated from the smaller intensity responses.

A few PMT's were studied for responses to magnetic fields and temperature changes. It was found that the pulse height loss due to a 1 gauss axial field is 5 to 15% for the three largest tubes; the 1.5 inch tube showed no effects from magnetic fields below 2 gauss. The E760 PMT's showed an order of magnitude less sensitivity to temperature than typical PMT's sensitivity of 1% per degree Celsius.

3.2.2 F2 Lead Glass Blocks

All lead-glass blocks were inspected visually for colloidal particles, bubbles, scratches and chips. The colloidal particles and bubbles could affect light transmission (the overall transmission of the blocks is discussed below). Small cracks could eventually lead to larger cracks and break the block. All scratches and chips were examined to make sure the integrity of each block was good since each block could be put under tremendous pressure (sections 3.1.4 and 3.2.3) and break due to imperfections. If chipping occurred during the manufacturing process, Cosmo Optics would smooth the chipped area and this would decrease the chance of breakage. Any chipped area greater than 1 cm caused a block to be rejected. Shallow scratches that were less than a few centimeters in length were accepted on all surfaces except where the PMT was to be attached.

Due to each block being a structural element of the overall calorimeter, the physical tolerances of the lead-glass blocks were kept stringent The lead-glass blocks were subject to tight tolerances, 0.08 mm. The length of a block was accepted up to 1 cm different than specified (table 3.1) as long as the front face (opposite side of where the PMT is attached) does not extend further than the wedge shell pocket and interfere with the front PVC panel (section 3.1.4).

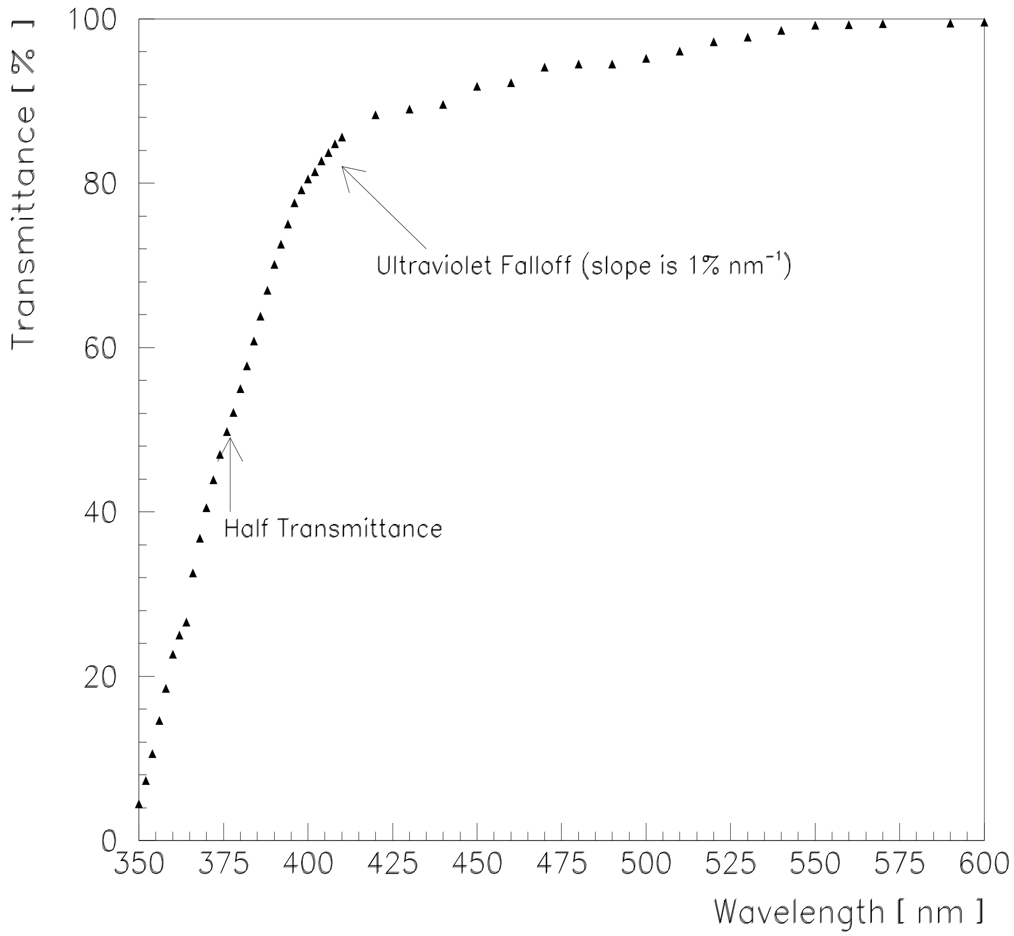

Figure 3.7: A typical lead-glass block transmission spectrum with the half transmittance and ultraviolet falloff (where the transmission spectrum's slope is 0.01 nm^{-1}) are shown.

The transmission of at least ten blocks from each melt (more than half of the blocks) was examined. The transmission measurements were done with a modified spectrophotometer (Appendix A). The spectrophotometer measurements were made at intervals of 2 nm, with an estimated error of ± 0.02 for each transmittance. A typical lead-glass block transmission spectrum is shown in figure 3.7. The lead-glass is nearly transparent for wavelengths greater than 500 nm.

Shape Number	Half Transmittance Wavelength (nm) Meas.	Corr.	Ultraviolet Falloff Wavelength (nm) Meas.	Corr.	Transmittance at Ultraviolet Falloff Meas.	Corr.
1	372.2	378.6	406.7	409.5	0.862	0.834
2	373.4	379.5	408.0	410.6	0.858	0.831
3	372.9	377.9	407.7	410.2	0.859	0.836
4	375.0	379.3	408.9	410.7	0.859	0.840
5	376.1	379.4	409.1	410.4	0.856	0.842
6	375.5	377.5	409.0	409.8	0.864	0.856
7	378.0	377.5	409.6	409.9	0.852	0.850
8	378.5	378.5	409.8	409.8	0.857	0.857
9	379.0	379.0	410.8	410.8	0.845	0.845
10	379.8	379.8	411.2	411.2	0.835	0.835
11	380.6	380.6	411.6	411.6	0.830	0.830
12	380.3	380.3	411.4	411.4	0.832	0.832
13	380.6	380.6	411.4	411.4	0.828	0.828
14	380.6	380.6	411.5	411.5	0.829	0.829
15	380.5	380.5	410.9	410.9	0.831	0.831
16	379.6	379.6	410.8	410.8	0.839	0.839
17	379.2	379.2	410.6	410.6	0.840	0.840
18	379.8	379.8	411.1	411.1	0.831	0.831
19	379.4	379.4	410.8	410.8	0.837	0.837
20	377.3	377.3	410.1	410.1	0.849	0.849

Table 3.5: The lead-glass blocks' transmission characterisitics as described in the text.

The average transmittance between 500 and 560 nm is 0.97. The average wavelength, for each of the twenty shapes, at which the the transmittance is 0.5, half transmittance, is shown in table 3.5. The differences of the half transmittances is caused by the different lengths. Half transmittances, corrected to a 50 cm length, are included in table 3.5. The length correction to the measured transmittance T_{meas} is

$$T_{corr}(\lambda) = [T_{meas}(\lambda)]^{\frac{50}{l}} \tag{3.2}$$

where l is the length of the block in cm. An ultraviolet falloff wavelength was calculated as the point where a fitted polynomial (between 374 and 424 nm) slope was equal to 0.01/nm (see figure 3.7). The average measured and length corrected ultraviolet falloff wavelength are shown with the measured transmittances at these wavelengths in table 3.5. Table 3.5 shows that the spectrophotometer measurements are consistent for all shapes (lengths). The average characteristics of all blocks measured by the spectrophotometer and corrected to a 50 cm length are 379 nm, 411 nm and 0.84 for half transmittance wavelength, wavelength and transmittance at ultraviolet falloff, respectively. The slope of the ultraviolet falloff was also calculated (straight line fit between 350 and 390 nm); the average corrected slope is 0.0405 nm^{-1}. The transmission spectra characteristics of all of the blocks are the same within the spectrophotometer's error.

3.2.3 Wedges

The wedge shell physical dimension tolerances are as stringent as the lead-glass blocks', 0.08 mm. This was necessary for the structural integrity of the calorimeter. The skins were required to be very flat so that there would be no gaps between wedges which would allow particles to escape detection.

Each wedge shell was measured on a granite table for the correct shape. Several wedge shells were tested to see if the shells would withstand the possible stresses that could occur during the construction process. Milled aluminum dummy blocks filled with lead shot were manufactured to represent a full set (20) of the correct shaped and weighted blocks. The dummy blocks were inserted into the pockets of a wedge shell and this wedge unit was subject to several tests. While on the granite table, the unit was subject to a 500 kg load (nearly twice the mass of a completed wedge) spread across one skin. The load was removed after several days. After removing the dummy blocks, the wedge shell was remeasured to see if the shape changed; there was no measurable change in shape. The dummy blocks were reinserted into the pockets and further tests involving movement of the wedge unit were conducted. Each wedge shell has two sets of two tapped holes for inserting eye-bolts; the eye-bolts allow for the wedge to be picked up by a crane. Testing both sets of holes, a crane lifted the wedge using the eye-bolts and then the wedge shell was remeasured; no change of shape was seen.

The wedge units could be picked up oriented with the back end of the unit downward. This orientation tested the mechanical supports that are attached to the fins to keep the blocks in the pockets; the tapering of the block keeps it from moving out the smaller end of the pocket. Another test to see if the wedge shells would deform or if the mechanical supports on the fins would fail was to change the vertical crane speed quickly (jerky motion). The mechanical supports worked and the wedge shell shape remained unchanged.

Inside each wedge unit are two harnesses: one electrical, for operating high voltage and signal cables, and one for the fiber optics (discussed in the next section). The high voltage cables are RG-58 and are cut to the appropriate lengths to reach each pocket. The signal cables are all the same length and are RG-174. All cables are connected by means of three block connectors (two for the high voltage) in the feed-through plate. All cables from every electrical harness were tested.

3.2.4 Fiber Optic System

Two major mixing bars and eighty minor mixing bars were made. The major mixing bars have eighty-one output fiber optic cables (9×9 grid) from which sixty-seven fibers have been chosen for the final gain monitoring system. The minor mixing bars are a smaller version with a 5×5 grid of output fiber optic cables for the twenty blocks inside the wedge and five spares. Twenty of the output fiber optic cables from the minor mixing bars are cut to the length needed to reach each pocket. The five spares are the length needed to reach the farthest pocket from the feed-through.

The major and minor mixing bars are $20 \times 5 \times 5$ cm^3 and $15 \times 4 \times 4$ cm^3, respectively, cut from lucite material. All sides are polished so that the light is internally reflected. The length of each bar is chosen so that the output end face is coherently illuminated.

The input light for the major mixing bar is from the xenon flashlamp by way of the elliptical reflector (see figure 3.5). An optic fiber is the light input for a minor mixing bar. In both cases the light is mixed enough over the length of the mixing bar that the intensities of all the output fibers are within 10% of each other. All of the fibers were tested for each mixing bar to identify defective and low intensity output fiber optic cables.

The fiber optic cables of the minor mixing bars were tested in the following manner. The first major mixing bar was only coupled to 10 output fibers and used with a flashlamp system during the cosmic ray muon test (section 4.1.2). One of these fibers was connected to a fiber optic feed-through similar to the the one used with each wedge unit. Each minor mixing bar was connected to the opposite side of the feed-through. Each fiber optic cable from the minor mixing bar was connected to a fiber optic snap connector (see section 3.3.1) glued to a 40 cm F2 lead-glass block. A PMT attached to the the opposite end of the block was used to measure the light intensity.

Typically, the individual fiber optic output intensity was spread about the average output intensity for the minor mixing bar; the spread of the twenty fiber optics is typically $\pm 10\%$. If the spread of the fiber optic output intensities was greater than 20%, the minor mixing bar was rejected. Also the lower average output intensity mixing bars were rejected. A fiber with an output intensity much less than the average for the mixing bar was replaced by one of the five spare optic fibers. Almost 5% of the designated fiber optic cables of the minor mixing bars were replaced by the spares.

The repeatability of connecting the fiber optic connections was tested. Each possible connection was tested: major mixing bar output fiber to the feed-through, the minor mixing bar input fiber to the feed-through, and the minor mixing bar output fiber to the snap connector attached to the lead-glass. All showed less than a 1% variation of the intensity, showing that the connection was repeatable and reliable. However, it was shown that the ends of the fiber optic cable had to be cleaned with alcohol and left to dry before connection to insure the small variation of the repeatability stated above. An uncleaned fiber optic could decrease the light intensity up to 12%. The minimum radius of curvature that an optic fiber could be bent before a significant decrease in light output intensity was determined to be ≈ 2 cm.

The major mixing bar was tested inside the flashlamp setup that was used in the final experimental setup. Each fiber optic output cable of the major mixing bar was tested using one minor mixing bar; the intensities were recorded.

3.3 Construction and Testing

The construction of the central calorimeter can be split into four parts: individual counters, flashlamp system, wedge units and the entire calorimeter. Nearly every step in building the calorimeter was subject to testing to assure that the quality of the calorimeter was good.

3.3.1 Individual Counters

After each PMT and lead-glass block had successfully passed the set of quality tests stated above in sections 3.2.1 and 3.2.2, the PMT was attached to the back face of the lead-glass block with Epotek 301 epoxy. A special gluing stand was made that held twenty lead-glass blocks oriented with the back faces upward. Centered upon the cleaned back face, several drops of epoxy were applied and then a PMT was pushed against the epoxy; pressure was applied until the epoxy covered the entire PMT face without bubbles. The epoxy needed twelve hours to cure after which a fiber optic snap connector was attached in one of the corners of the back face.

The PMT is wrapped in a μ–metal shield two and a half turns. The μ–metal is 0.1 mm thick and 10 cm wide. The lead-glass block is wrapped in one layer of 3 mil white paper. The paper serves two purposes: to cushion the counter inside the wedge units and to reflect Čerenkov light not reflected internally (see section C.4 for Monte Carlo and experimental effects of the paper wrapping). The front face has more than one layer; the flaps from the side faces are folded and taped across the front face. The back face is not covered by the paper.

Each assembled counter was tested with through going cosmic ray muons and a flashlamp, as will be discussed in section 4.1.2. The test was for determining the initial voltages while checking the construction of the counters, optical *goodness* of the PMT–lead-glass glue joint and fiber optic snap connector.

3.3.2 Flashlamp System

The fiber optic output apparatus for optically coupling the output fibers to the lucite block is the same for the major and minor mixing bars. A piece of PVC was milled to the rectangular shape to fit on an end of the major (minor) mixing bar,

$1 \times 5 \times 5$ cm^3 ($1 \times 4 \times 4$ cm^3), and eighty-one (twenty-five) holes were drilled through it in a 9×9 (5×5) grid. The holes are slightly larger than an uncladded optic fiber. The eighty-one (twenty-five) fiber optics were put into the holes and glued into place using epoxy. When the epoxy had dried, the ends of all the fibers, which extended pass the end of the piece of PVC, were polished until even with the PVC face. The PVC–fiber optic apparatus is attached to the lucite mixing bar with epoxy.

The major mixing bar front face sits at a focal point of the flashlamp system's ellipsoidal reflector. Between the reflector and major mixing bar is a filter wheel. The filter wheel is controlled remotely and allows for four settings: no filtration, stop all light, filters to allow the blue or green components of the spectrum. The flashlamp system (flashlamp bulb and electronics, reflector, major mixing bar and filter wheel) is enclosed inside of a box. The minor mixing bars are inside PVC pipe. The ends of the PVC pipes are closed by end caps with holes cut for the fiber optic cables. An opaque epoxy, RTV, was used to fill the end cap holes and hold the fiber optic cables in place while reducing stress to the overall mixing bar apparatus.

3.3.3 Wedges

After a wedge shell had been determined to have the correct shape, the wedge pockets cleaned and twenty counters from different rings successfully tested with cosmic ray muons, the twenty counters were inserted into the wedge shell's pockets. The wedge and counters were entered into a data base program before the actual insertion; the data base also contains the operating voltage, gain curves for each counter and results of the cosmic ray muon test (section 4.1.2). The insertion of the counters was done carefully to avoid tearing the paper, which could easily be torn upon the wedge shell's stiffing strips or the fins. If the paper wrapping was ripped, the counter was removed, wrapped in a new piece of paper and reinserted; about 10% of the counters had to be rewrapped with paper.

If the counter was successfully inserted into the correct pocket, a mechanical support was attached via a clamp to the fin separating the counter from the next lower counter; the ring 1 mechanical support was connected to the wedge shell end plate. A set screw attached to the mechanical support was tightened against each counter until either the pocket's and counter's tapers did not allow the counter to move further or the front of the counter extended no more that a few millimeters past the end of the pocket's fins.

An operating electrical harness was then attached to the counters. At each position there were three connections of the electrical harness to the PMT; the signal cable, high voltage and ground. The electrical harness was attached to the inner side of one of the skins. The fiber optic harness was attached to the opposite inner skin of the wedge shell. The correct fiber optic, as determined from tests discussed in section 3.2.4, was then connected to each counter at the snap connector. The input fiber optic cable of the minor mixing bar was then connected to the fiber optic feed-through. The ends of the unused fiber optic cables were covered so as not to introduce any extraneous light sources inside the wedge.

The feed-through plate was glued to the downstream outer panel using the opaque epoxy. The outer panels were put on loosely and a front panel was put in place before connecting an outside test harness, electrical cables and fiber optic cable, to the feed-through plate and covering the entire wedge with a dark blanket. Each counter was turned on to its operating voltage and examined with a flashlamp signal to check and see if all connections, electrical and optical, had been made successfully. If all counters were found functioning, the outside test harness was removed and the outer panels' screws were tightened. The opaque epoxy was then used to attach the front PVC panel and fill all possible gaps around the outer panels.

After the epoxy had dried, the wedges were checked for light leaks, i.e. if ambient light could be seen by the counters. The test harness was again attached to the feed-through plate and the counters were turned on at their operating voltages while the fiber optic cable feed-through was covered. The only signals expected were from dark current, cosmic rays and light leaks. By monitoring which counters experienced a continuous signal, the location of a light leak could be found. A flashlight and dark cover would be alternated over an area to see a change in counter response in order to locate the light leak. Light leaks caused by gaps between panels were fixed by using the opaque epoxy. Black paint was used when a light leak was found at one of the laser welds. The paint was allowed to dry in the laser weld divot and then sanded off the wedge skin (no extra material between wedges). The wedge was picked up by a crane to allow for light leak testing on every side of the wedge.

3.3.4 Calorimeter

After a wedge was determined to be light tight and operational, it was placed on the massive support rings. The wedges were at first hung at the bottom of the calorimeter and then built up evenly on each side until the last few wedges were hung into place. Each wedge is held in place by several bolts and positioned with some set crews which also allowed for the wedge to be moved radially.

A crane-supported transport mechanism was used for most wedges. The wedge transport mechanism used a vacuum system, with an air pumping system, to lift the wedges. The wedge was rotated to the correct orientation before being placed upon the previously positioned wedge and connected to the support rings.

After a wedge was positioned on the support rings, the counters in the wedge were tested again at operating voltage looking for light leaks and the response to the flashlamp was compared to earlier tests. When all the wedges were connected to the support rings and positioned, the counters were tested again. The flashlamp system was placed upon the calorimeter raft and sixty-four of the eighty-one fiber optic cables were connected to the wedges' fiber optic feed-throughs after considering the relative output intensity of the fiber optic cables and the relative average light output of the minor mixing bars. The fiber optic cables of the major mixing bar with larger intensities were connected to the minor mixing bars with the smaller average intensities (intensity determination is in section 3.2.4). Again counters from each wedge were tested at operating voltages to check and see if the counters' responses were acceptable, i.e. on scale.

Some of the inner detectors were inserted and connected to the calorimeter support structure. Before transporting the calorimeter apparatus to the experimental area, the signal cables were connected to the wedges. Sixty-four bundles of twenty signal cables, that were to be connected to the twenty Level I summer modules (section 2.9) in the experimental area, were woven correctly before transport: sixty-four bundles of twenty cables to twenty bundles of sixty-four cables.

A transport frame was attached to the raft. The calorimeter apparatus and support structure were lifted by a crane (by the transport frame) and loaded onto a semi-trailer flat bed truck. The calorimeter was transported two miles and another crane unloaded the raft support apparatus through an access hatch to the experimental area. The transport frame was removed. Every counter was again tested with the flashlamp signal; only one counter was found to be not working.

The five air caster system allowed the raft to be maneuvered in the experimental area. The gas jet and the rest of the inner detectors were inserted and connected to the raft support apparatus. The detectors were connected to the electronics located in the experimental area; the operating high voltage cables were connected to the wedges and the woven signal cable bundles were connected to the Level I summer modules. The entire apparatus and electronic racks were moved into place using the air caster system. The raft was then aligned with the beam pipe using four motorized screw jacks and eight hydraulic cylinders.

Once in place, the calorimeter counters were all tested, one at a time, with the data acquisition electronics. Tests were done confirming that the counters were operational and that the acquisition electronic channels were labelled correctly. The flashlamp controls, on/off and filter wheel, were also connected to the data acquisition.